Comparative Hybrid Hartree-Fock-DFT Calculations of WO$_2$-Terminated Cubic WO$_3$ as Well as SrTiO$_3$, BaTiO$_3$, PbTiO$_3$ and CaTiO$_3$ (001) Surfaces

R. I. Eglitis [1],*, **Juris Purans** [1] and **Ran Jia** [1,2]

1   Institute of Solid State Physics, University of Latvia, 8 Kengaraga Street, LV1063 Riga, Latvia; purans@cfi.lu.lv (J.P.); jiaran@jlu.edu.cn (R.J.)

2   Laboratory of Theoretical and Computational Chemistry, Institute of Theoretical Chemistry, Jilin University, Changchun 130023, China

*   Correspondence: rieglitis@gmail.com; Tel.: +371-26426703

Abstract: We performed, to the best of our knowledge, the world's first first-principles calculations for the WO$_2$-terminated cubic WO$_3$ (001) surface and analyzed the systematic trends in the WO$_3$, SrTiO$_3$, BaTiO$_3$, PbTiO$_3$ and CaTiO$_3$ (001) surface ab initio calculations. According to our first principles calculations, all WO$_2$ or TiO$_2$-terminated WO$_3$, SrTiO$_3$, BaTiO$_3$, PbTiO$_3$ and CaZrO$_3$ (001) surface upper-layer atoms relax inwards towards the crystal bulk, while all second-layer atoms relax upwards. The only two exceptions are outward relaxations of first layer WO$_2$ and TiO$_2$-terminated WO$_3$ and PbTiO$_3$ (001) surface O atoms. The WO$_2$ or TiO$_2$-terminated WO$_3$, SrTiO$_3$, BaTiO$_3$, PbTiO$_3$ and CaTiO$_3$ (001) surface-band gaps at the Γ–Γ point are smaller than their respective bulk-band gaps. The Ti–O chemical bond populations in the SrTiO$_3$, BaTiO$_3$, PbTiO$_3$ and CaTiO$_3$ bulk are smaller than those near the TiO$_2$-terminated (001) surfaces. Conversely, the W–O chemical bond population in the WO$_3$ bulk is larger than near the WO$_2$-terminated WO$_3$ (001) surface.

Keywords: Ab initio calculations; ABO$_3$ (001) surfaces; WO$_3$; hybrid exchange–correlation functionals

1. Introduction

Throughout the last 20 years the SrTiO$_3$, BaTiO$_3$, PbTiO$_3$ and CaTiO$_3$ (001) surfaces have been broadly explored theoretically and experimentally [1–10]. At the same time, to the best of our knowledge, there are no reports of ab initio calculations dealing with the atomic relaxation and electronic structure of the pristine WO$_2$-terminated WO$_3$ (001) surface in the cubic perovskite-like structure. Nevertheless, a large amount of experimental studies exist dealing with WO$_3$ (001) surfaces [11–14]. Recent theoretical studies have been devoted, for example, to hydrogen adsorption on the WO$_3$ (001) surface [15], understanding the water splitting process on the WO$_3$ (001) surface [16], and H$_2$O adsorption on the WO$_3$ (001) surface [17].

BaTiO$_3$, PbTiO$_3$ and CaTiO$_3$ perovskites have attracted huge fundamental interest in these materials mostly for their phase transitions. Historically the ABO$_3$ perovskites were highly promising low-cost energy materials. They have been used for numerous optoelectronic and photonic device applications [18]. SrTiO$_3$ perovskite thin films are important for a large amount of technologically important applications [19,20]. For example, they are used for catalysis, optical wave guides, high-capacity memory cells as well as substrates for high-temperature cuprate superconductor growth [19,20]. Barium titanate (BaTiO$_3$) is an excellent photorefractive material [18]. Ferroelectric PbTiO$_3$ thin films have been applied to large numbers of electronic devices, such as non-volatile memory FET [19] and Si monolithic ultrasonic sensors [18]. CaTiO$_3$ is used worldwide in technologically important electronic ceramic materials [18]. Tungsten trioxide (WO$_3$) and its thin films exhibit a large number of novel properties useful for high-technology applications [21]. In particular, WO$_3$ undergoes phase transitions, which are explored for their potential in

industrial applications, display systems and microelectronics [21]. It is worth noting that the predictive power of ab initio calculations makes possible the design of new materials for high-technology applications on paper. Nowadays, consumer electronics mostly use lithium-ion batteries containing $LiCoO_2$ cathode, which was discovered in 1980 by J. Goodenough, one of the 2019 Nobel Prize winners for Chemistry [22]. The experimentally detected $LiCoO_2$ average intercalation voltage is 4.0–4.1 V [23]. Based on ab initio calculations by Eglitis and Borstel [24–26], it was demonstrated that a novel $Li_2CoMn_3O_8$ battery cathode material can lead to a high-energy lithium-ion battery working at the 5 V regime.

The $SrTiO_3$, $BaTiO_3$, $PbTiO_3$ and $CaTiO_3$ perovskite cubic unit cells contain five atoms. The A type atom (A = Sr, Ba, Pb or Ca) has the coordinates (0, 0, 0), and it is located in the cube corner position. The Ti atom has the coordinates $(\frac{1}{2}, \frac{1}{2}, \frac{1}{2})$, and it is located in the cube body center position. The 3 O atoms have the coordinates $(\frac{1}{2}, \frac{1}{2}, 0)$, $(\frac{1}{2}, 0, \frac{1}{2})$, $(0, \frac{1}{2}, \frac{1}{2})$, and they are located in the cube face centered positions. All $SrTiO_3$, $BaTiO_3$, $PbTiO_3$ and $CaTiO_3$ cubic perovskites have the same space group Pm3m with the space group number equal to 221. WO_3 in its cubic perovskite-like structure has exactly the same space group as $ATiO_3$ perovskites Pm3m, and also the same space group number 221. The only striking difference between the $SrTiO_3$, $BaTiO_3$, $PbTiO_3$ and $CaTiO_3$ cubic perovskites as well as WO_3 in its cubic perovskite-like structure is that WO_3 has an empty A cation position. Thereby, the cubic perovskite-like unit cell of WO_3 contain only four atoms.

The objective of the reported here work was to carry out first-principles calculations for WO_2-terminated polar WO_3 (001) surfaces in the cubic perovskite-like structure. We compared our WO_2-terminated WO_3 (001) surface-atomic and electronic-structure ab initio calculations with our results for the related structure TiO_2-terminated $SrTiO_3$, $BaTiO_3$, $PbTiO_3$ and $CaTiO_3$ cubic perovskite (001) surfaces. We carefully compared our calculation results for all five of our calculated materials and detected systematic common trends. The results for WO_2-terminated WO_3 and TiO_2-terminated $SrTiO_3$, $BaTiO_3$, $PbTiO_3$ and $CaTiO_3$ (001) surfaces were summarized and analysed in a way easily readable for a broad audience of scientists.

2. Computational Methods and Surface Models

In order to carry out ab initio DFT-B3LYP or DFT-B3PW calculations, we employed the CRYSTAL computer program package [27]. Unlike the plane-wave codes widely employed in many previous studies [28,29], the CRYSTAL code [27] uses localized Gaussian-type basis sets. In our calculations, we adopted the basis sets (BS) developed for $SrTiO_3$, $BaTiO_3$ and $PbTiO_3$ in [30]. The Hay–Wadt small-core, effective-core pseudopotentials (ECP) were adopted for Ca and Ti atoms [31–33]. The small-core ECPs replaced only the inner-core orbitals, while orbitals for subvalence electrons as well as for valence electrons were calculated self-consistently. Oxygen atoms were treated with the all-electron BS. Finally, for the W atom we used BS developed by Cora et al. [34]. Our calculations were performed by means of the B3LYP [35] or B3PW [36–38] hybrid exchange–correlation functionals. For all WO_3, $SrTiO_3$, $BaTiO_3$, $PbTiO_3$ and $CaTiO_3$ materials we performed the reciprocal space integration with an $8 \times 8 \times 8$ and $8 \times 8 \times 1$ extension of Pack–Monkhorst mesh for the bulk and (001) surfaces of these materials. The CRYSTAL computer program package [27] makes possible the calculation of isolated 2D slabs perpendicular to the Oz direction. In order to compare the performance of different exchange–correlation functionals and choose the best method for our calculations, we calculated the $SrTiO_3$, $SrZrO_3$, $BaZrO_3$, MgF_2 and CaF_2 bulk Γ–Γ band gaps [30,39–42] (Table 1 and Figure 1). The experimentally detected $SrTiO_3$, $SrZrO_3$, $BaZrO_3$, MgF_2 and CaF_2 bulk band gaps at the Γ-point are mentioned in Table 1 for comparison purposes as well as depicted in Figure 1 [43–47].

Table 1. By means of different exchange–correlation functionals calculated $SrTiO_3$, $SrZrO_3$, $BaZrO_3$, MgF_2 and CaF_2 bulk Γ–Γ band gaps (eV). Experimental bulk band gaps at the Γ-point are listed for comparison.

Method	SrTiO$_3$ [30]	SrZrO$_3$ [39]	BaZrO$_3$ [40]	MgF$_2$ [41]	CaF$_2$ [42]
Experiment	3.75 [43]	5.6 [44]	5.3 [45]	13.0 [46]	12.1 [47]
B3PW	3.96	5.30	4.93	9.48	10.96
B3LYP	3.89	5.31	4.79	9.42	10.85
HF	12.33	13.54	12.96	19.65	20.77
PWGGA	2.31	3.53	3.24	6.94	8.51
PBE	2.35	3.52	-	6.91	8.45
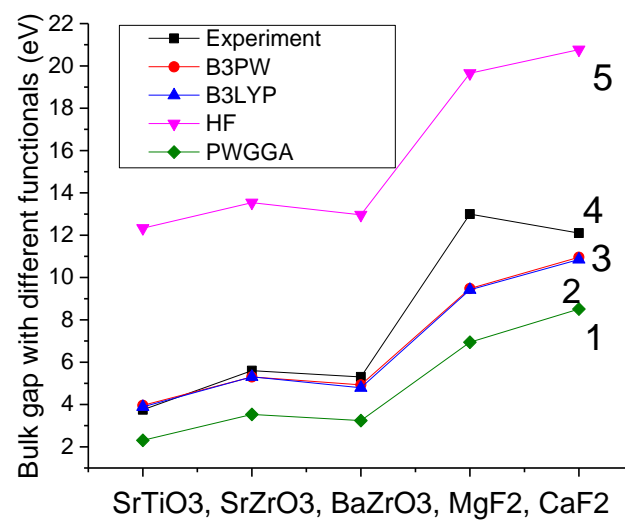
Figure 1. Ab initio calculated and experimentally measured bulk Γ–Γ band gaps for $SrTiO_3$, $SrZrO_3$, $BaZrO_3$, MgF_2 and CaF_2 obtained by means of different exchange–correlation functionals: (1) PWGGA; (2) B3LYP; (3) B3PW; (4) Experiment; (5) HF.

As can be seen in Table 1, the ab initio Hartree-Fock (HF) calculations, for all five our calculated materials, very strongly overestimate the experimental band gap at Γ-point. Namely, the HF method most strongly (3.29 times) overestimate the experimental $SrTiO_3$ bulk Γ–Γ band gap. Even HF calculated MgF_2 bulk Γ–Γ band gap overestimates the experimental value 1.51 times (Table 1 and Figure 1).

From another side, as we can see from Table 1 and Figure 1, the generalized gradient approximations (GGA) to the density functional theory (DFT) systematically and considerably underestimate the experimental Γ–Γ bulk band gap in our calculated ABO_3 perovskites as well as MgF_2 and CaF_2. For example, the PWGGA (6.94 eV) and PBE (6.91 eV) calculated MgF_2 bulk band gap at Γ-point is 1.87 and 1.88 times, respectively, smaller than the experimental MgF_2 bulk Γ–Γ band gap value of 13.0 eV [37].

To obtain the best possible results, we performed our WO_3, $SrTiO_3$, $BaTiO_3$, $PbTiO_3$ and $CaTiO_3$ bulk and (001) surface calculations by means of the B3PW [36–38] or B3LYP [35] hybrid exchange–correlation functionals. The hybrid functional incorporates a portion of exact exchange energy density from HF theory (20%) while the rest of the exchange–correlation part is a mixture of different approaches (both exchange and correlation). It is obvious, that the B3PW and B3LYP hybrid exchange–correlation functionals, since they are a superposition of HF and DFT methods as implemented in the CRYSTAL computer code [27], allowed us to achieve as good an agreement as possible between the first principles calculated and the experimentally detected Γ–Γ band gaps for WO_3, $SrTiO_3$, $BaTiO_3$, $PbTiO_3$ and $CaTiO_3$ bulk and their (001) surfaces.

In our ab initio calculations we used WO_2-terminated WO_3 as well as TiO_2-terminated $SrTiO_3$, $BaTiO_3$, $PbTiO_3$ and $CaTiO_3$ (001) slabs containing 9 alternating layers. First our calculated WO_3 (001) slab was terminated by WO_2 planes from both sides (WO_2–O–WO_2_O–WO_2–O–WO_2–O–WO_2) from a 19-atom supercell (Figure 2). Another of our calculated $SrTiO_3$, $BaTiO_3$, $PbTiO_3$ and $CaTiO_3$ (001) slabs was terminated by TiO_2 planes from both sides (TiO_2–AO–TiO_2–AO–TiO_2–AO–TiO_2–AOvTiO_2) and consisted of a 23-atom supercell (Figure 3). Both our calculated slabs were non-stoichiometric and had unit-cell equations W_5O_{14} as well as $A_4Ti_5O_{14}$, respectively. To analyse the chemical bonds, effective atomic charges and covalency effects for WO_3 and $ATiO_3$ perovskite bulk and (001) surfaces, we used the well-known Mulliken population analysis [48–52].
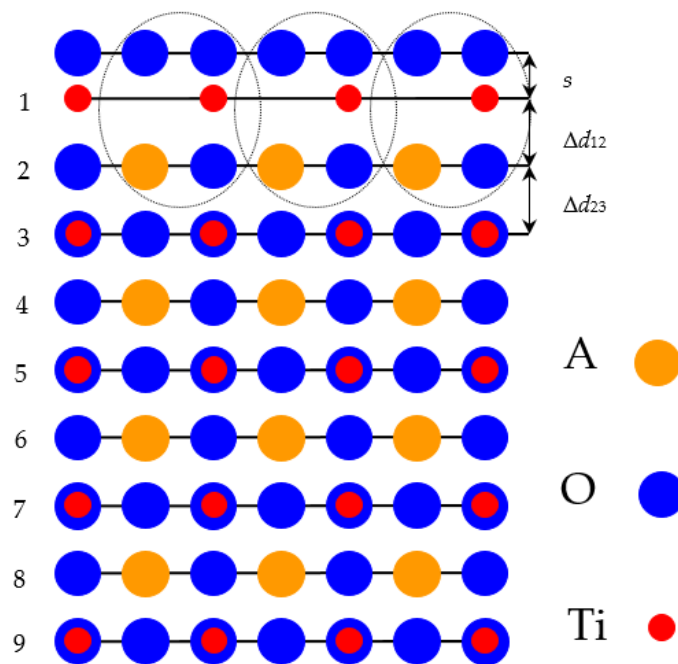

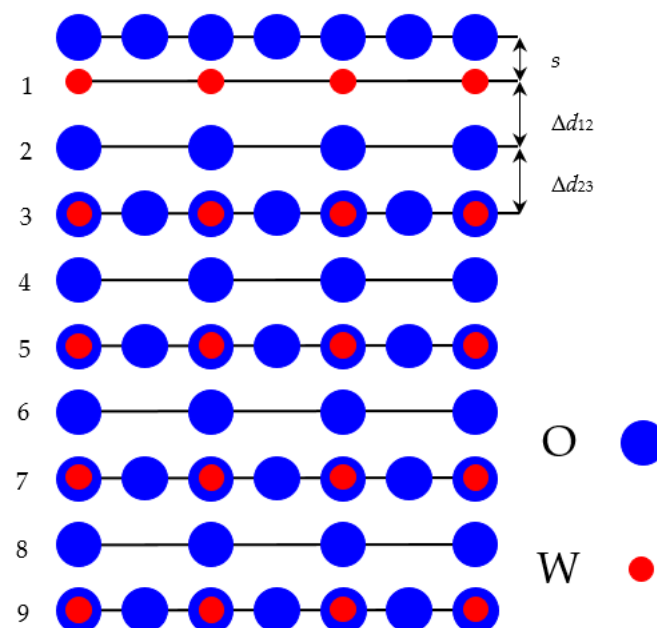**Figure 2.** Side view of the nine-layer TiO_2-terminated $ATiO_3$ perovskite (001) surface.

Figure 3. Side view of the nine-layer WO_2-terminated WO_3 polar (001) surface.

3. Ab initio Calculation Results for WO_3, $SrTiO_3$, $BaTiO_3$, $PbTiO_3$ and $CaTiO_3$ Bulk

As a starting point, by means of the hybrid B3LYP exchange–correlation functional, we calculated the cubic WO_3 bulk lattice constant (3.775 Å). Our calculated cubic WO_3 constant (3.775 Å) was only slightly larger than the experimental value of a_0 = 3.71–3.75 Å [51] (Table 2); nevertheless, it was in almost perfect agreement with the earlier calculation result for the WO_3 cubic structure bulk lattice constant calculated by the full-potential linear muffin-tin (FP-LMTO) code equal to 3.78 Å [52]. Our B3PW-calculated $SrTiO_3$ bulk lattice constant (3.904 Å) was only slightly overestimated with respect to the experimental $SrTiO_3$ bulk lattice constant (3.89 Å) extrapolated to 0 K [53] (Table 2). Our ab initio calculation of the $BaTiO_3$ bulk lattice constant (4.008 Å) was in an outstanding agreement with the experimental value of 4.00 Å [53–55]. Our B3PW-calculated $PbTiO_3$ bulk lattice constant (3.936 Å) [54–56] was only 0.86% under the experimental value of 3.97 Å [57]. Finally, our calculated $CaTiO_3$ bulk lattice constant (3.851 Å) was 1.17% smaller than the experimentally detected (3.8967 Å) [58–60] (Table 2).

Table 2. Our ab initio-calculated and experimentally measured WO_3, $SrTiO_3$, $BaTiO_3$, $PbTiO_3$ and $CaTiO_3$ bulk lattice constants [51–60].

Material	Method	Theory	Experiment
WO_3	B3LYP	3.775	3.71–3.75 [51]
	FP-LMTO	3.78 [52]	
$SrTiO_3$	B3PW	3.904	3.89 [53]
$BaTiO_3$	B3PW	4.008	4.00 [53,54]
$PbTiO_3$	B3PW	3.936	3.97 [54,57]
$CaTiO_3$	B3PW	3.851	3.8967 [58–60]

Our ab initio B3LYP-calculated effective atomic charges for the WO_3 bulk were (+3.095e) for the W atom, and (−1.032e) for each of the three O atoms (Table 3). Our B3LYP-calculated effective W atomic charge (+3.095e) was almost two times smaller than the generally accepted classical ionic charge for the W(+6e) atom. In addition, our calculated effective atomic charge for the O (−1.032e) atom was almost two times smaller than the generally accepted O atom classical ionic charge (−2e). In addition, for the $SrTiO_3$, $BaTiO_3$, $PbTiO_3$ and $CaTiO_3$ perovskites, our calculated A atomic charges (+1.871e, +1.797e, +1.354e and +1.782e, respectively) were considerably smaller than those of the classical Sr, Ba, Pb, Ca atom ionic charges (+2e) (Table 3) [61–66]. Our B3PW-calculated O atom Mulliken charges in $SrTiO_3$, $BaTiO_3$, $PbTiO_3$ and $CaTiO_3$ perovskites (−1.407e, −1.388e, −1.232e and −1.371e, respectively) are also at least 29.65% smaller than the classical ionic O atomic charge (−2e) [67–69]. Finally, our ab initio-calculated $SrTiO_3$, $BaTiO_3$, $PbTiO_3$ and $CaTiO_3$ Ti atomic charges (+2.351e, +2.367e, +2.341e and 2.330e) are more than one-and-a-half times smaller than the formal Ti atom ionic charge (+4e). Our calculated chemical bond population between W and O atoms in WO_3 bulk (0.142e) is approximately one-and-a-half times larger than the Ti–O atom chemical bond population in $SrTiO_3$, $BaTiO_3$, $PbTiO_3$ and $CaTiO_3$ perovskites (+0.088e, +0.098e, +0.098e and +0.084e, respectively).

Our B3LYP-calculated WO_3 bulk Γ–Γ band gap (4.95 eV) overestimated by 1.21 eV the experimental direct WO_3 bulk band gap value at Γ-point of 3.74 eV [70] (Table 4). Moreover, our B3PW-calculated bulk Γ–Γ band gaps for $SrTiO_3$, $BaTiO_3$, $PbTiO_3$ and $CaTiO_3$ perovskites (3.96 eV, 3.55 eV, 4.32 eV and 4.18 eV, respectively) were always slightly overestimated with respect to the experimentally measured direct band gap values at Γ-point for $SrTiO_3$, $BaTiO_3$, $PbTiO_3$ and $CaTiO_3$ perovskites (3.75 eV [43], 3.2 eV [71], 3.4 eV [72] and 3.5 eV [73], respectively) (Table 4).

Table 3. Our calculated atomic charges $Q(e)$ as well as bond populations $P(e)$ in WO_3, $SrTiO_3$, $BaTiO_3$, $PbTiO_3$ and $CaTiO_3$ bulk materials.

Bulk Materials		WO_3	$SrTiO_3$	$BaTiO_3$	$PbTiO_3$	$CaTiO_3$
Ion	Property	B3LYP	B3PW	B3PW	B3PW	B3PW
A	Q	-	+1.871	+1.797	+1.354	+1.782
	P	-	−0.010	−0.034	+0.016	+0.006
O	Q	−1.032	−1.407	−1.388	−1.232	−1.371
	P	+0.142	+0.088	+0.098	+0.098	+0.084
B	Q	+3.095	+2.351	+2.367	+2.341	+2.330

Table 4. Ab initio-calculated WO_3, $SrTiO_3$, $BaTiO_3$, $PbTiO_3$ and $CaTiO_3$ bulk band gaps for the cubic phase at the Γ–Γ point. Our B3LYP and B3PW calculations were compared with the relevant experimental data.

Crystal	Method	Optical Bulk Band Gap at Γ–Γ Point	
		Ab Initio Calculations	Experimental Results
WO_3	B3LYP	4.95	3.74 [70]
$SrTiO_3$	B3PW	3.96	3.75 [43]
$BaTiO_3$	B3PW	3.55	3.2 [71]
$PbTiO_3$	B3PW	4.32	3.4 [72]
$CaTiO_3$	B3PW	4.18	3.5 [73]

4. Ab Initio Calculation Results for the WO_2-Terminated WO_3 as Well as TiO_2-Terminated $SrTiO_3$, $BaTiO_3$, $PbTiO_3$ and $CaTiO_3$ (001) Surfaces

Our B3LYP- or B3PW-calculated atomic displacements for the WO_2-terminated WO_3 and the TiO_2-terminated $SrTiO_3$, $BaTiO_3$, $PbTiO_3$ and $CaTiO_3$ (001) surface upper-three or two layers are presented in Table 5. According to our B3LYP or B3PW calculations, all atoms of the first (upper) surface layer relaxed inwards, while all second-layer atoms relaxed outwards (Table 5). The only two exceptions to this systematic trend were the outward relaxation of the first layer O atom of the WO_2-terminated WO_3 (001) surface (+0.42% of a_0) and the outward relaxation of the TiO_2-terminated $PbTiO_3$ (001) surface first-layer O atom by (0.31% of a_0) (Table 5). The first layer metal atom relaxation magnitudes range from −1.71% of a_0 for the TiO_2-terminated $CaTiO_3$ (001) surface to −3.08% of a_0 for the TiO_2-terminated $BaTiO_3$ (001) surface (Table 5). The first- and second-layer metal atom displacement magnitudes for WO_2-terminated WO_3 and TiO_2-terminated $SrTiO_3$, $BaTiO_3$, $PbTiO_3$ and $CaTiO_3$ (001) surfaces were always considerably larger than the respective first- and second-layer O atom displacement magnitudes (Table 5).

Our B3LYP-calculated surface rumpling amplitude s (the relative displacement of an oxygen atom relative to the metal atom in the upper surface layer) for WO_2-terminated WO_3 (001) surface (+2.49) is in qualitative agreement with our B3PW-calculated surface rumpling amplitudes s for TiO_2-terminated $BaTiO_3$, $PbTiO_3$, $CaTiO_3$ and $SrTiO_3$ (001) surfaces (+2.73, +3.12, +1.61 and +2.12, respectively) (Table 6). Our B3PW-calculated surface rumpling amplitude s for TiO_2-terminated $SrTiO_3$ (001) surface (+2.12) is in fair agreement with available RHEED (+2.6 [74]) and LEED (+2.1 ± 2 [75]) experimental data (Table 6). Unfortunately, our B3PW-calculated interlayer distance Δd_{12} for the TiO_2-terminated $SrTiO_3$ (001) surface (−5.80) had the opposite sign to the experimentally measured RHEED (+1.8 [74]) and LEED (+1 ± 1 [67]) interlayer distances (Table 6). Finally, our B3PW-calculated interlayer distance Δd_{23} for the TiO_2-terminated $SrTiO_3$ (001) surface (+3.55) is in qualitative agreement with the RHEED experiment result (+1.3), but had the opposite sign to that of the LEED experimental result (−1 ± 1). Nevertheless, it is worth noting that the RHEED (+1.3) and the LEED experiments (−1 ± 1) had opposite signs for the interlayer distance Δd_{23} (Table 6).

Table 5. WO_2-terminated WO_3 as well as TiO_2-terminated $SrTiO_3$, $BaTiO_3$, $PbTiO_3$ and $CaTiO_3$ (001) surface atom relaxation for upper-three surface layers (in percent of the bulk lattice constant).

Surfaces, (001)		WO_3	$SrTiO_3$	$BaTiO_3$	$PbTiO_3$	$CaTiO_3$
Layer	Ion	WO_2-Term.	TiO_2-Term.	TiO_2-Term.	TiO_2-Term.	TiO_2-Term.
Method		B3LYP	B3PW	B3PW	B3PW	B3PW
1	B	−2.07	−2.25	−3.08	−2.81	−1.71
	O	+0.42	−0.13	−0.35	+0.31	−0.10
2	A	Absent	+3.55	+2.51	+5.32	+2.75
	O	+0.11	+0.57	+0.38	+1.28	+1.05
3	B	−0.01	-	-	-	-
	O	0.00	-	-	-	-

Table 6. Our B3LYP- or B3PW-calculated surface rumplings s and relative displacements Δd_{ij} between the three near-surface planes for the WO_2-terminated WO_3 and the TiO_2-terminated $BaTiO_3$, $PbTiO_3$, $CaTiO_3$ and $SrTiO_3$ (001) surfaces as a percent of the bulk material lattice constant. The available experimental data are listed for comparison purposes.

Material	Method	WO_2- or TiO_2-Terminated (001) Surface		
		s	Δd_{12}	Δd_{23}
WO_3	B3LYP	+2.49	-	-
$BaTiO_3$	B3PW	+2.73	−5.59	+2.51
$PbTiO_3$	B3PW	+3.12	−8.13	+5.32
$CaTiO_3$	B3PW	+1.61	−4.46	+2.75
$SrTiO_3$	B3PW	+2.12	−5.80	+3.55
	RHEED exp. [74]	+2.6	+1.8	+1.3
	LEED exp. [75]	+2.1 ± 2	+1 ± 1	−1 ± 1

We started the discussion of the electronic structure of WO_2-terminated WO_3 and TiO_2-terminated $SrTiO_3$, $BaTiO_3$, $PbTiO_3$ and $CaTiO_3$ (001) surfaces with an analysis of charge redistribution in the top-three surface planes (Table 7). The ab initio-calculated atomic displacements, bond populations between the nearest metal and oxygen atoms and the effective atomic charges are collected in Table 7. For example, the effective static atomic charges on WO_2-terminated WO_3 as well as TiO_2-terminated $SrTiO_3$, $BaTiO_3$, $PbTiO_3$ and $CaTiO_3$ (001) surface upper-layer W and Ti atoms are always reduced in comparison to the bulk WO_3, $SrTiO_3$, $BaTiO_3$, $PbTiO_3$ and $CaTiO_3$ crystal charges (−0.312e, −0.06e, −0.06e, −0.062e and −0.052e, respectively). We recently observed a similar effect: the reduction of surface upper-layer metal atomic charges near the ReO_2-terminated ReO_3 and the ZrO_2-terminated $SrZrO_3$, $BaZrO_3$, $PbZrO_3$ and $CaZrO_3$ (001) surfaces [76]. According to our ab initio calculations, the largest upper-layer metal atom displacement was observed for the TiO_2-terminated $BaTiO_3$ (001) surface Ba atom (−0.123 Å). Nevertheless, the TiO_2-terminated $PbTiO_3$ (001) surface second-layer Pb atom outward displacement (+0.209 Å) was even larger.

Our B3PW-calculated $SrTiO_3$, $BaTiO_3$, $PbTiO_3$ and $CaTiO_3$ bulk Ti-O chemical bond covalency (+0.088e, +0.098e, +0.098e and +0.084e, respectively) were always smaller than near the TiO_2-terminated $SrTiO_3$, $BaTiO_3$, $PbTiO_3$ and $CaTiO_3$ (001) surfaces (0.118e, 0.126e, 0.114e, 0.114e, respectively) (Table 8 and Figure 4). Just opposite situation was obtained for the WO_3 crystal: the B3LYP-calculated W-O chemical bond population in the WO_3 bulk (0.142e) was larger than near the WO_2-terminated WO_3 (001) surface (0.108e) (Table 8 and Figure 4). Nevertheless, it is worth noting that the W–O chemical bond population between the W atom on the top layer of WO_2-terminated WO_3 (001) surface and the O atom on the

second layer (0.278*e*) is the largest one (Table 8), which was in agreement with our previous B3LYP calculations dealing with ReO$_2$-terminated ReO$_3$ (001) surfaces [76].

Table 7. Our B3LYP- or B3PW-calculated atomic shift magnitudes *D* (in *Å*) as well as the effective atomic charges *Q* (in *e*) and nearest atomic chemical bond populations *P* (in *e*) for the WO$_2$- and TiO$_2$-terminated WO$_3$, SrTiO$_3$, BaTiO$_3$, PbTiO$_3$ and CaTiO$_3$ (001) surfaces.

WO$_2$ and TiO$_2$-Term. (001) Surfaces			WO$_3$	SrTiO$_3$	BaTiO$_3$	PbTiO$_3$	CaTiO$_3$
Layer	**Property**	**Ion**	**WO$_2$-Ter.**	**TiO$_2$-Ter.**	**TiO$_2$-Ter.**	**TiO$_2$-Ter.**	**TiO$_2$-Ter.**
1	D	B	−0.078	−0.088	−0.123	−0.111	−0.066
	Q		+2.783	+2.291	+2.307	+2.279	+2.278
	P		+0.108	+0.118	+0.126	+0.114	+0.114
	D	O	+0.016	−0.005	−0.014	+0.012	−0.004
	Q		−1.146	−1.296	−1.280	−1.184	−1.267
	P		−0.014	−0.014	−0.038	+0.044	+0.016
2	D	A	-	+0.139	+0.101	+0.209	+0.106
	Q		-	+1.850	+1.767	+1.275	+1.754
	P		-	−0.008	−0.030	+0.008	+0.006
	D	O	+0.004	+0.022	+0.015	+0.050	+0.041
	Q		−0.925	−1.365	−1.343	−1.167	−1.324
	P		+0.064	+0.080	+0.090	+0.080	+0.086
3	D	B	−0.0004	-	-	-	-
	Q		+3.001	+2.348	+2.365	+2.335	+2.326
	P		+0.144	+0.096	+0.104	+0.108	+0.090
	D	O	0.000	-	-	-	-
	Q		−1.037	−1.384	−1.371	−1.207	−1.354
	P		−0.032	−0.010	−0.034	+0.018	+0.008

Table 8. Our B3LYP or B3PW calculated W–O or Ti–O chemical bond populations for WO$_3$, SrTiO$_3$, BaTiO$_3$, PbTiO$_3$ and CaTiO$_3$ bulk and for WO$_2$- or TiO$_2$-terminated (001) surfaces (in *e*).

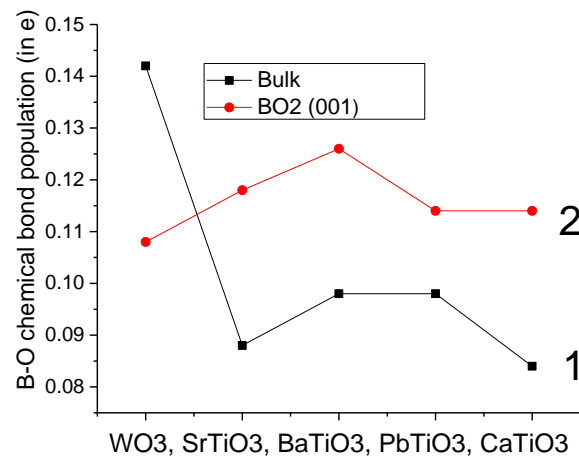| Material	Method	W-O or Ti-O Chemical Bond Populations	
		Bulk	**WO$_2$, TiO$_2$-Term. (001)**
WO$_3$	B3LYP	+0.142	+0.108 (W(I)—O(I))
		+0.142	+0.278 (W(I)—O(II))
SrTiO$_3$	B3PW	+0.088	+0.118
BaTiO$_3$	B3PW	+0.098	+0.126
PbTiO$_3$	B3PW	+0.098	+0.114
CaTiO$_3$	B3PW	+0.084	+0.114

Figure 4. Our ab initio-calculated bulk (1) as well as BO_2-terminated (001) surface (2). B–O chemical bond populations (in *e*) for WO_3, $SrTiO_3$, $BaTiO_3$, $PbTiO_3$ and $CaTiO_3$.

As can be seen in Table 9 and Figure 5, our B3LYP- or B3PW-calculated WO_3, $SrTiO_3$, $BaTiO_3$, $PbTiO_3$ and $CaTiO_3$ bulk band gaps at the Γ–Γ point were always reduced near the WO_2- or TiO_2-terminated WO_3, $SrTiO_3$, $BaTiO_3$, $PbTiO_3$ and $CaTiO_3$ (001) surfaces. The B3PW-calculated $SrTiO_3$ bulk band gap at Γ–Γ point near the TiO_2-terminated $SrTiO_3$ (001) surface at Γ–Γ point was reduced only by 0.01 eV. At the same time, our B3LYP-calculated WO_3 bulk band gap (4.95 eV) at the Γ–Γ point near the WO_2-terminated WO_3 (001) surface was reduced by 3.79 eV to 1.16 eV (Table 9 and Figure 5).

Table 9. B3LYP- or B3PW-calculated Γ–Γ band gaps for WO_3, $SrTiO_3$, $BaTiO_3$, $PbTiO_3$ and $CaTiO_3$ bulk as well as their WO_2 or TiO_2-terminated (001) surfaces.

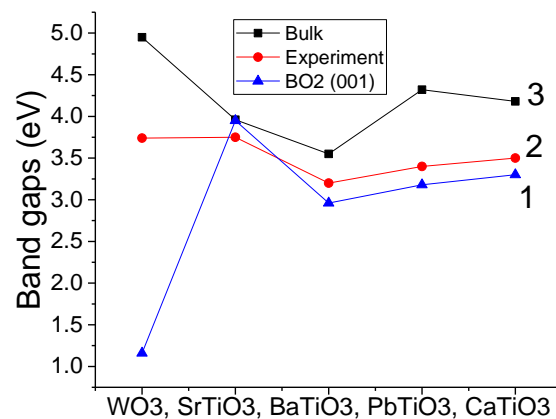| Material	Method	Calculated Band Gap at Γ–Γ Point	
		Bulk	**WO_2, TiO_2-Term. (001)**
WO_3	B3LYP	4.95	1.16
$SrTiO_3$	B3PW	3.96	3.95
$BaTiO_3$	B3PW	3.55	2.96
$PbTiO_3$	B3PW	4.32	3.18
$CaTiO_3$	B3PW	4.18	3.30

Figure 5. Our ab initio-calculated WO_2-terminated WO_3 and TiO_2-terminated $SrTiO_3$, $BaTiO_3$, $PbTiO_3$ and $CaTiO_3$ (001) surface Γ–Γ band gaps (line 1). Experimentally measured bulk Γ–Γ band gaps (line 2). Our ab initio-calculated WO_3, $SrTiO_3$, $BaTiO_3$, $PbTiO_3$ and $CaTiO_3$ bulk Γ–Γ band gaps (line 3).

5. Conclusions

For the first principles-calculated WO_2- or TiO_2-terminated WO_3, $SrTiO_3$, $BaTiO_3$, $PbTiO_3$ and $CaTiO_3$ (001) surfaces, as a rule, all first-layer surface atoms relax inwards, whereas all second-layer surface atoms relax upwards. The only two exceptions from this systematic trend are the upward relaxation of WO_2- or TiO_2-terminated WO_3 and $PbTiO_3$ (001) surface first-layer O atoms. As a result of our ab initio-calculated atomic relaxation, TiO_2-terminated $SrTiO_3$, $BaTiO_3$, $PbTiO_3$ and $CaTiO_3$ (001) surfaces exhibited a reduction of the interlayer distance Δd_{12} (-5.80, -5.59, -8.13, -4.46% of a_0, respectively) as well as an expansion of Δd_{23} ($+3.55$, $+2.51$, $+5.32$, $+2.75\%$ of a_0, respectively). It is worth noting that after geometry optimization, it is very useful to perform ab initio molecular dynamics computations to ensure the stability of the structures over time [77].

The changes in the interlayer distances between the first and second layer (Δd_{12}) were always larger than between the second and third layer (Δd_{23}) for all our calculated perovskites $SrTiO_3$, $BaTiO_3$, $PbTiO_3$ and $CaTiO_3$.

The Ti–O chemical bond population in $SrTiO_3$, $BaTiO_3$, $PbTiO_3$ and $CaTiO_3$ bulk was always smaller than near their TiO_2-terminated (001) surface (see Figure 4). In contrast, the W–O chemical bond population in the WO_3 bulk ($0.142e$) was larger than near the WO_2-terminated WO3 (001) surface ($0.108e$). Nevertheless, the largest W–O chemical bond population, according to our ab initio calculations, is between the W atom located on the WO_2-terminated WO_3 (001) surface and the second-layer O atom ($0.278e$). It was worth noting, that also for the related material ReO_3, according to our calculations [76], the situation was similar. Namely, the Re–O chemical bond population in the ReO_3 bulk ($0.212e$) was larger than near the ReO_2-terminated ReO_3 (001) surface ($0.170e$). Nevertheless, the Re–O chemical bond population between the Re atom located on the ReO_2-terminated ReO_3 (001) surface upper-layer and O atom located on the ReO_2-terminated ReO_3 (001) surface second layer was the largest ($0.262e$).

According to our B3LYP or B3PW calculations, the WO_3, $SrTiO_3$, $BaTiO_3$, $PbTiO_3$ and $CaTiO_3$ bulk Γ–Γ band gap values (4.95, 3.96, 3.55, 4.32, 4.18 eV, respectively) were always reduced with respect to the bulk near the WO_2- or TiO_2-terminated WO_3, $SrTiO_3$, $BaTiO_3$, $PbTiO_3$ and $CaTiO_3$ (001) surfaces (1.16, 3.95, 2.96, 3.18, 3.30 eV, respectively) (see Figure 5).

Author Contributions: All authors equally contributed to the performed ab initio calculations as well as to the preparation of the manuscript. All authors have read and agreed to the published version of the manuscript.

Institutional Review Board Statement: Not applicable.

Informed Consent Statement: Not applicable.

Data Availability Statement: Not applicable.

Conflicts of Interest: The authors declare no conflict of interest.

References

1. Solokha, V.; Garai, D.; Wilson, A.; Duncan, D.A.; Thakur, P.K.; Hingerl, K.; Zegenhagen, J. Water splitting on Ti-oxide-terminated $SrTiO_3$ (001). *J. Phys. Chem. C* **2019**, *123*, 17232–17238. [CrossRef]
2. Saghayezhian, M.; Sani, S.M.R.; Zhang, J.D.; Plummer, E.W. Rumpling and enhanced covalency at the $SrTiO_3$ (001) surface. *J. Phys. Chem. C* **2019**, *123*, 8086–8091. [CrossRef]
3. Foo, G.S.; Hood, Z.D.; Wu, Z.L. Shape effect undermined by surface reconstruction: Ethanol dehydrogenation over shape-controlled $SrTiO_3$ nanocrystals. *ACS Catal.* **2018**, *8*, 555–565. [CrossRef]

4.   Ryu, G.H.; Lewis, N.P.; Kotsonis, G.N.; Maria, J.P.; Dickey, E.C. Crystallization behavior of amorphous BaTiO$_3$ thin films. *J. Mater. Sci.* **2020**, *55*, 8793–8801. [CrossRef]

5.   Heifets, E.; Eglitis, R.I.; Kotomin, E.A.; Maier, J.; Borstel, G. Ab initio modeling of surface structure for SrTiO$_3$ perovskite. *Phys. Rev. B* **2001**, *64*, 235417. [CrossRef]

6.   Ananyev, M.V.; Porotnikova, N.M.; Eremin, V.A.; Kurumchin, E.K. Interaction of O$_2$ with LSM-YSZ Composite Materials and Oxygen Spillover Effect. *ACS Catal.* **2021**, *11*, 4247–4262. [CrossRef]

7.   Piskunov, S.; Eglitis, R.I. First principles hybrid DFT calculations of BaTiO$_3$/SrTiO$_3$ (001) interface. *Solid State Ionics* **2015**, *274*, 29–33. [CrossRef]

8.   Sternlicht, H.; Rheinheimer, W.; Dunin-Borkowski, R.E.; Hoffmann, M.J.; Kaplan, W.D. Characterization of grain boundary disconnections in SrTiO$_3$ part I: The dislocation component of grain boundary disconnections. *J. Mater. Sci.* **2019**, *54*, 3694–3709. [CrossRef]

9.   Borstel, G.; Eglitis, R.I.; Kotomin, E.A.; Heifets, E. Modelling of defects and surfaces in perovskite ferroelectrics. *Phys. Stat. Sol. B* **2003**, *236*, 253–264. [CrossRef]

10.   Eglitis, R.; Kruchinin, S.P. Ab initio calculations of ABO$_3$ perovskite (001), (011) and (111) nano-surfaces, interfaces and defects. *Modern Phys. Lett. B* **2020**, *34*, 2040057. [CrossRef]

11.   Dixon, R.A.; Williams, J.J.; Morris, D.; Rebane, J.; Jones, F.H.; Egdell, R.G.; Downes, S.W. Electronic states at oxygen deficient WO$_3$ (001) surfaces: A study by resonant photoemission. *Surf. Sci.* **1998**, *399*, 199–211. [CrossRef]

12.   Jones, F.H.; Rawlings, K.; Foord, J.S.; Egdell, R.G.; Pethica, J.B.; Wanklyn, B.M.R.; Parker, S.C.; Oliver, P.M. An STM study of surface structures on WO$_3$ (001). *Surf. Sci.* **1996**, *359*, 107–121. [CrossRef]

13.   Bringaus, R.D.; Höchst, H.; Shanks, H.R. Hydrogen on WO$_3$ (001). *Surf. Sci.* **1981**, *111*, 80–86. [CrossRef]

14.   Jones, F.H.; Dixon, R.A.; Brown, A. Observation of reduced (1 × 1) terraces on WO$_3$ (001) surfaces using scanning tunneling microscopy. *Surf. Sci.* **1996**, *369*, 343–350. [CrossRef]

15.   Wang, F.; Valentin, C.D.; Pacchioni, G. DFT study of hydrogen adsorption on the monoclinic WO$_3$ (001) surface. *J. Phys. Chem. C* **2012**, *116*, 10672–10679. [CrossRef]

16.   Teuch, T.; Klüner, T. Understanding the water splitting mechanism on WO$_3$ (001)—A theoretical approach. *J. Phys. Chem. C* **2019**, *123*, 28233–28240. [CrossRef]

17.   Albanese, E.; Valentin, C.D.; Pacchioni, G. H$_2$O adsorption on WO$_3$ and WO$_{3-x}$ (001) surfaces. *ACS Appl. Mater. Interfaces* **2017**, *9*, 23212–23221. [CrossRef]

18.   Dawber, M.; Rabe, K.M.; Scott, J.F. Physics of thin-film ferroelectric oxides. *Rev. Mod. Phys.* **2005**, *77*, 1083–1130. [CrossRef]

19.   Auciello, O.; Scott, J.F.; Ramesh, R. The physics of ferroelectric memories. *Phys. Today* **1998**, *51*, 22–27. [CrossRef]

20.   Goniakowski, J.; Finnochi, F.; Noguera, C. Polarity of oxide surfaces and nanostructures. *Rep. Progr. Phys.* **2008**, *71*, 016501. [CrossRef]

21.   Granqvist, C.G. Electrochromic tungsten oxide films: Review of progress 1993–1998. *Solar Energy Mater. Solar Cells* **2000**, *60*, 201–262. [CrossRef]

22.   Mizushima, K.; Jones, P.C.; Wiseman, P.J.; Goodenough, J.B. LixCoO$_2$ (0 < x < −1): A new cathode material for batteries of high energy density. *Mater. Res. Bull.* **1980**, *15*, 783–789. [CrossRef]

23.   Ohzuku, T.; Ueda, A. Solid-State Redox Reactions of LiCoO$_2$ (R3m) for 4 Volt Secondary Lithium Cells. *J. Electrochem. Soc.* **1994**, *141*, 2972–2977. [CrossRef]

24.   Eglitis, R.I.; Borstel, G. Towards a practical rechargeable 5 V Li ion battery. *Phys. Stat. Sol. A* **2005**, *202*, R13–R15. [CrossRef]

25.   Eglitis, R.I. Theoretical prediction of the 5 V rechargeable Li ion battery using Li$_2$CoMn$_3$O$_8$ as a cathode. *Phys. Scr.* **2015**, *90*, 094012. [CrossRef]

26.   Eglitis, R. Ab initio calculations of Li$_2$(Co, Mn)O$_8$ solid solutions for rechargeable batteries. *Int. J. Mod. Phys. B* **2019**, *33*, 1950151. [CrossRef]

27.   Saunders, V.R.; Dovesi, R.; Roetti, C.; Causa, N.; Harrison, N.M.; Orlando, R.; Zicovich-Wilson, C.M. *CRYSTAL-2009 User Manual*; University of Torino: Turin, Italy, 2009.

28.   Cohen, R.E. Periodic slab LAPW computations for ferroelectric BaTiO$_3$. *J. Phys. Chem. Solids* **1996**, *57*, 1393–1396. [CrossRef]

29.   Cohen, R.E. Surface effects in ferroelectrics: Periodic slab computations for BaTiO$_3$. *Ferroelectrics* **1997**, *194*, 323–342. [CrossRef]

30.   Piskunov, S.; Heifets, E.; Eglitis, R.I.; Borstel, G. Bulk properties and electronic structure of SrTiO$_3$, BaTiO$_3$, PbTiO$_3$ perovskites: An ab initio HF/DFT study. *Comput. Mater. Sci.* **2004**, *29*, 165–178. [CrossRef]

31.   Hay, P.J.; Wadt, W.R. Ab initio effective core potentials for molecular calculations. Potentials for the transition metal atoms Sc to Hg. *J. Chem. Phys.* **1985**, *82*, 270–283. [CrossRef]

32.   Hay, P.J.; Wadt, W.R. Ab initio effective core potentials for molecular calculations. Potentials for main group elements Na to Bi. *J. Chem. Phys.* **1985**, *82*, 284–298.

33.   Hay, P.J.; Wadt, W.R. Ab initio effective core potentials for molecular calculations. Potentials for K to Au including the outermost core orbitals. *J. Chem. Phys.* **1985**, *82*, 299–310. [CrossRef]

34.   Cora, F.; Patel, A.; Harrison, N.M.; Dovesi, R.; Catlow, C.R.A. An ab initio Hartree-Fock study of the cubic and tetragonal phases of bulk tungsten trioxide. *J. Am. Chem. Soc.* **1996**, *118*, 12174–12182. [CrossRef]

35.   Lee, C.; Yang, W.; Parr, R.G. Development of the Colle-Salvetti correlation-energy formula into a functional of the electron density. *Phys. Rev. B* **1988**, *37*, 785–789. [CrossRef] [PubMed]

36. Perdew, J.P.; Wang, Y. Accurate and simple density functional for the electronic exchange energy: Generalized gradient approximation. *Phys. Rev. B* **1986**, *33*, 8800–8802. [CrossRef]

37. Perdew, J.P.; Wang, Y. Erratum: Accurate and simple density functional for the electronic exchange energy: Generalized gradient approximation. *Phys. Rev. B* **1989**, *40*, 3399. [CrossRef]

38. Perdew, J.P.; Wang, Y. Accurate and simple analytic representation of the electron-gas correlation energy. *Phys. Rev. B* **1992**, *45*, 13244–13249. [CrossRef] [PubMed]

39. Eglitis, R.I.; Rohlfing, M. First-principles calculations of the atomic and electronic structure of SrZrO$_3$ and PbZrO$_3$ (001) and (011) surfaces. *J. Phys. Condens. Matter* **2010**, *22*, 415901. [CrossRef]

40. Eglitis, R.I.; Popov, A.I. Systematic trends in (001) surface ab initio calculations of ABO$_3$ perovskites. *J. Saudi Chem. Soc.* **2018**, *22*, 459–468. [CrossRef]

41. Vassilyeva, A.F.; Eglitis, R.I.; Kotomin, E.A.; Dauletbekova, A.K. Ab initio calculations of MgF$_2$ (001) and (011) surface structure. *Phys. B* **2010**, *405*, 2125–2127. [CrossRef]

42. Shi, H.; Eglitis, R.I.; Borstel, G. Ab initio calculations of the CaF$_2$ electronic structure and *F* centers. *Phys. Rev. B* **2005**, *72*, 045109. [CrossRef]

43. Van Benthem, K.; Elsasser, C.; French, R.H. Bulk electronic structure of SrTiO$_3$: Experiment and theory. *J. Appl. Phys.* **2001**, *90*, 6156–6164. [CrossRef]

44. Lee, Y.S.; Lee, J.S.; Noh, T.W.; Byun, D.Y.; Yoo, K.S.; Yamaura, K.; Takayama-Muromachi, E. Systematic trends in the electronic structure parameters of the 4d transition-metal oxides SrMO$_3$ (M = Zr, Mo, Ru and Rh). *Phys. Rev. B* **2003**, *67*, 113101. [CrossRef]

45. Robertson, J. Band offsets of wide-band-gap oxides and implications for future electronic devices. *J. Vacuum. Sci. Technol. B* **2000**, *18*, 1785–1791. [CrossRef]

46. Lisitsyn, V.M.; Lisitsyna, L.A.; Popov, A.I.; Kotomin, E.A.; Abuova, F.U.; Akilbekov, A.; Maier, J. Stabilization of primary mobile radiation defects in MgF$_2$ crystals. *Nucl. Instrum. Methods B* **2016**, *374*, 24–28. [CrossRef]

47. Rubloff, G.W. Far-Ultraviolet Reflectance Spectra and the electronic structure of ionic crystals. *Phys. Rev. B* **1972**, *5*, 662–684. [CrossRef]

48. Bochicchio, R.C.; Reale, H.F. On the nature of crystalline bonding: Extension of statistical population analysis to two- and three-dimensional crystalline systems. *J. Phys. B At. Mol. Opt. Phys.* **1993**, *26*, 4871–4883. [CrossRef]

49. Eglitis, R.I.; Piskunov, S. First principles calculations of SrZrO$_3$ bulk and ZrO$_2$-terminated (001) surface *F* centers. *Comput. Condens. Matter* **2016**, *7*, 1–6. [CrossRef]

50. Jia, W.; Vikhnin, V.S.; Liu, H.; Kapphan, S.; Eglitis, R.; Usvyat, D. Critical effects in optical response due to charge transfer vibronic excitions and their structure in perovskite-like systems. *J. Lumin.* **1999**, *83*, 109–113. [CrossRef]

51. Balászi, C.; Farkas-Jahnke, M.; Kotsis, I.; Petrás, L.; Pfeifer, J. The observation of cubic tungsten trioxide at high-temperature dehydration of tungsten acid hydrate. *Solid State Ion.* **2001**, *141–142*, 411–416. [CrossRef]

52. Cora, F.; Stachiotti, M.G.; Catlow, C.R.A.; Rodriguez, C.O. Transition Metal Oxide Chemistry: Electronic Structure Study of WO$_3$, ReO$_3$ and NaWO$_3$. *J. Phys. Chem. B* **1997**, *101*, 3945–3952. [CrossRef]

53. Hellwege, K.H.; Hellwege, A.M. *Ferroelectrics and Related Substances*; Landolt-Bornstein, New Series, Group III; Springer: Berlin/Heidelberg, Germany, 1969; Volume 3.

54. Eglitis, R.I.; Vanderbilt, D. Ab initio calculations of BaTiO$_3$ and PbTiO$_3$ (001) and (011) surface structures. *Phys. Rev. B* **2007**, *76*, 155439. [CrossRef]

55. Eglitis, R.I. Ab initio calculations of SrTiO$_3$, BaTiO$_3$, PbTiO$_3$, CaTiO$_3$, SrZrO$_3$, PbZrO$_3$ and BaZrO$_3$ (001), (011) and (111) surfaces as well as *F* centers, polarons, KTN solid solutions and Nb impurities therein. *Int. J. Mod. Phys. B* **2014**, *28*, 1430009. [CrossRef]

56. Eglitis, R.I. Comparative first-principles calculations of SrTiO$_3$, BaTiO$_3$, PbTiO$_3$ and CaTiO$_3$ (001), (011) and (111) surfaces. *Ferroelectrics* **2015**, *483*, 53–67. [CrossRef]

57. Mabud, S.A.; Glazer, A.M. Lattice parameters and birefringence in PbTiO$_3$ single crystals. *J. Appl. Cryst.* **1979**, *12*, 49–53. [CrossRef]

58. Eglitis, R.I.; Vanderbilt, D. Ab initio calculations of the atomic and electronic structure of CaTiO$_3$ (001) and (011) surfaces. *Phys. Rev. B* **2008**, *78*, 155420. [CrossRef]

59. Eglitis, R.I. Comparative ab initio calculations of SrTiO$_3$ and CaTiO$_3$ polar (111) surfaces. *Phys. Stat. Sol. B* **2015**, *252*, 635–642. [CrossRef]

60. Ali, R.; Yashima, M. Space group and crystal structure of the perovskite CaTiO$_3$ from 296 to 1720 K. *J. Solid State Chem.* **2005**, *178*, 2867–2872. [CrossRef]

61. Eglitis, R.I.; Kleperis, J.; Purans, J.; Popov, A.I.; Jia, R. Ab initio calculations of CaZrO$_3$ (011) surfaces: Systematic trends in polar (011) surface calculations of ABO$_3$ perovskites. *J. Mater. Sci.* **2020**, *55*, 203–217. [CrossRef]

62. Piskunov, S.; Eglitis, R.I. Comparative ab initio calculations of SrTiO$_3$/BaTiO$_3$ and SrZrO$_3$/PbZrO$_3$ (001) heterostructures. *Nucl. Instr. Methods Phys. Res. B* **2016**, *374*, 20–23. [CrossRef]

63. Eglitis, R.I. First-principles calculations of BaZrO$_3$ (001) and (011) surfaces. *J. Phys. Condens. Matter* **2007**, *19*, 356004. [CrossRef]

64. Eglitis, R.I.; Purans, J.; Popov, A.I.; Jia, R. Systematic trends in YAlO$_3$, SrTiO$_3$, BaTiO$_3$, BaZrO$_3$ (001) and (111) surface ab initio calculations. *Int. J. Mod. Phys. B* **2019**, *33*, 1950390. [CrossRef]

65. Eglitis, R.I.; Vanderbilt, D. First-principles calculations of atomic and electronic structure of SrTiO$_3$ (001) and (011) surfaces. *Phys. Rev. B* **2008**, *77*, 195408. [CrossRef]

66. Eglitis, R.I.; Popov, A.I. Comparative ab initio calculations for ABO$_3$ perovskite (001), (011) and (111) surfaces as well as YAlO$_3$ (001) surfaces and *F* centers. *J. Nano Electron. Phys.* **2019**, *11*, 01001. [CrossRef]

67. Eglitis, R.I. Theoretical modelling of the energy surface (001) and topology of CaZrO$_3$ perovskite. *Ferroelectrics* **2008**, *483*, 75–85. [CrossRef]

68. Eglitis, R.I.; Piskunov, S.; Zhukovskii, Y.F. Ab initio calculations of PbTiO$_3$/SrTiO$_3$ (001) heterostructures. *Phys. Stat. Sol. C* **2016**, *13*, 913–920. [CrossRef]

69. Eglitis, R.I.; Popov, A.I. Ab initio calculations for the polar (001) surfaces of YAlO$_3$. *Nucl. Instr. Methods Phys. Res. B* **2018**, *434*, 1–5. [CrossRef]

70. Koffyberg, F.P.; Dwight, K.; Wold, A. Interband transitions of semiconducting oxides determined from photoelectrolysis spectra. *Solid State Commun.* **1979**, *30*, 433–437. [CrossRef]

71. Wemple, S.H. Polarization Fluctuations and the Optical-Absorption Edge in BaTiO$_3$. *Phys. Rev. B* **1970**, *2*, 2679–2689. [CrossRef]

72. Peng, C.H.; Chang, J.F.; Desu, S. Optical Properties of PZT, PLZT and PNZT Thin Films. *Mater. Res. Soc. Symp. Proc.* **1991**, *243*, 21–26. [CrossRef]

73. Ueda, K.; Yanagi, H.; Noshiro, R.; Hosono, H.; Kawazoe, H. Vacuum ultraviolet reflectance and electron energy loss spectra of CaTiO$_3$. *J. Phys. Condens. Matter* **1998**, *10*, 3669–3677. [CrossRef]

74. Hikita, T.; Hanada, T.; Kudo, M.; Kawai, M. Structure and electronic state of the TiO$_2$ and SrO-terminated SrTiO$_3$ (100) surface. *Surf. Sci.* **1993**, *287*, 377–381. [CrossRef]

75. Bickel, N.; Schmidt, G.; Heinz, K.; Muller, K. Ferroelectric relaxation of the SrTiO$_3$ (100) surface. *Phys. Rev. Lett.* **1989**, *62*, 2009–2011. [CrossRef] [PubMed]

76. Eglitis, R.I.; Purans, J.; Gabrusenoks, J.; Popov, A.I.; Jia, R. Comparative ab initio calculations of ReO$_3$, SrZrO$_3$, BaZrO$_3$, PbZrO$_3$ and CaZrO$_3$ (001) surfaces. *Crystals* **2020**, *10*, 745. [CrossRef]

77. Car, R.; Parrinello, M. Unified approach for molecular dynamics and density-functional theory. *Phys. Rev. Lett.* **1985**, *55*, 2471–2474. [CrossRef]